Laboratoire Bordelais de Recherche en Informatique
UMR 5800 - Université Bordeaux I, 351, cours de la Libération,
33405 Talence CEDEX, France

Research Report RR-1454-09

Strasbourg Juvenile Collection: Computer Assisted Anthropology for the Anterior Fontanelle Reconstruction and Size Evaluation

Desbarats,P., Gueorguieva,S., Synave,R.
Coqueugniot,H. and Dutailly,B.

Mars, 2009

Strasbourg Juvenile Collection: Computer Assisted Anthropology for the Anterior Fontanelle Reconstruction and Size Evaluation

Contents

Abstract

Laser scan acquisition, reconstruction and size evolution measurement of the anterior fontanelle are presented for the private osteology collection of the chair of anatomy in the Faculty of Medicine at Strasbourg.
Two main results are presented. The first one regards the skull cap fixed error acquisition and reconstruction. The second one concerns the evaluation of the heterogeneity of the fontanelle closure processes.

1 Introduction

Digital anthropology provides powerful tools for investigations and "revisiting" exiting studies and theories on human evolution and in particular, the skull juvenile osteology. The general framework of the current research is the application of the modern medical imaging techniques to the geometric morphometrics. In a more precise way, we are interested in retrieval of geometric computer models of anatomical shapes for some collection of specimens and the simulation of the geometric morphometric analysis through digital image processing.

In a traditional way [1], morphometrics uses a full arsenal of multivariate statistical tools to describe patterns of shape variation. First, sets of morphological variables including distances, distance ratios, and/or angles gathered to sample the shape of the object are identified. Next, multivariate statistical analysis typically including principal components analysis, factor analysis, canonical variates analysis and etc., is performed in order to determine shape differences and variations. Finally, the focus is put on geometric interpretation of the extracted patterns. The basic drawback of this approach is that pertinent geometric information about the biological structure of interest could be neglected. For instance, the same set of distance measures could be obtained from different shapes because the location of where the distances are made relative to one another is not included in the data. Moreover, graphical representations of the shape is usually impossible to generate as long as the relative spatial geometric relationships are not preserved (sets of linear distances is often insufficient to capture the geometry of the original shape). Recently, a new track, called geometric morphometrics, [10], emerged. Object shape is defined in terms of functional and geometric shape features using homologous sets of outlines and landmarks. Using 3D contact laser digitizers scanners and/or Computer Tomography scanners, digital images of specimens are produced including precise outline and landmark positions. This makes possible registration and multivariate analysis of curves and regions on the input objects and thus supporting the 3D reconstruction and the visualisation of the shape and size variation. Our long-term aim is to further take advantage of modern techniques in range image acquisition, segmentation and reconstruction [8]. Indeed, till now all the morphometric measurements are applied on the registered outline and landmark positions. No morphometric analysis is performed on the reconstructed image of the initial object shape as a whole. For this purpose, the entire pipeline from the data acquisition to the image reconstruction and the shape and size variation

calculation should be refashioned. A new research field, we call **digital morphometrics**, could emerge and make possible to perform morphological studies as analysis on different types of supports such as collections of specimens, real or synthetic objects or computer geometric models, for different types of shape features as distances, angles, outlines, landmarks, surface or volume features, according to different types of metrics as euclidean metrics [5], geodesics metrics [6, 11] or multivariate statistical metrics [10].

An immediate application of this approach will be experienced in the current research for the paleoanthropology investigation of the anterior fontanelle. Four intermediate stages are identified:

- Object feature definition defining the anterior fontanelle.

  In this phase, depending on the geometric properties of the anterior fontanelle, the morphometric relevant data are specified following familiar to physical anthropologist expertise. The purpose is to establish the best object orientation for the subsequent data range acquisition and registration of the chosen morphometric outlines and landmarks.

- Data acquisition and anterior fontanelle reconstruction.

  The acquisition of the object boundary is done using surface laser scanner [12]. The registration produces a computer geometric model of the anterior fontanelle in the form of a triangular mesh model.

- Digital morphometric analysis.

  At this point, the digital morphometrics analysis starts up with interactive landmark editing. Outlines are brought forward for inspection in order to readjust their positions. Morphometric data measurements are performed according to a chosen protocol using chosen metrics and applied on chosen shape features of the computer geometric model. Multivariate statistical shape analysis is performed using geodesic discrete distance measurements in the reconstructed range images [13]. The underlying basic idea is to assess geodesic shortest path (in contrast to linear distance Euclidean shortest path) and using a discrete Gauss curvature evaluator [11].

- Reproduction and validation of the results.

  The visualization of the numerical model along with the map of geodesics path delimiting the morphometric data in use is generated in order to obtain visual control of the shape feature relocation and the shape and size variation. Further, a result validation step is foreseen based on comparison of the calculated numerical rates with known evaluations of the considered morphometric data.

Each of these items will be developed in the following sections. First the specimen collection supporting the present study of the anterior fontanelle and the corresponding morphometric characteristics will be considered. Next, the experimental platform and the digital morphometric analysis will be examined.

Further, the quantitative results will be provided and finally the entire retrieval pipeline will be discussed.

2 Juvenile collection of Strasbourg

The juvenile human skull collection housed in the chair of anatomy in the Faculty of Medicine at Strasbourg is under the responsibility of Professor J.-L. Khan. The specimens were prepared by anatomists between 1872 and 1918. Half of the specimens were born in Strasbourg, 34% in Alsace or bordering regions and the rest came from Germany. Biological data are available: sex is known for most specimens and calendar ages are known with a precision of one month, one week or sometimes one day.

Previous investigations of the osteology collection of Strasbourg could be found in [7, 3]. In the current research the studied sample of specimens is presented in Table 1. The specimen sex is denoted as F for female, M for male and I for indeterminate. The age is given in days, month and years denoted as d, m and y filed from civil records. In case of missing records, the dental age is evaluated. In Table 2 the age sample is summarized. The integer digits correspond to the number of specimens for each sex composition.

3 Osteology of anterior fontanelle

3.1 Shape feature definition

The frontal bone is ossified from two primary centers, each half of the bone ossifies from a single center which appears between 6 and 7 weeks of the foetal life and is situated above the supra orbital margin as illustrated in Fig. 1. From each of these centers, ossification extends upward to form the corresponding half of the squama, and backward to form the orbital plate. The spine is ossified from a pair of secondary centers, on either side of the middle line. Similar centers appear in the nasal part and the zygomatic process. For details see in [9].
At birth the frontal bone is composed of two pieces, which are separated from each other by the metopic suture. They are also separated from the parietal bones by the diamond-shaped anterior fontanelle. This membranous gap allows the development and the growth of the brain and the skull. From a sample of 138 known-aged children, it has been suggested [2] that the oldest child with an anterior fontanelle was around 2.5 years old. Even if the correlation with age is not so high, the closure of the anterior fontanelle was used, along with the feature of the inner ear, to estimate the age of death of the Mojokerto *Homo erectus* infant [4].

In order to evaluate the anterior fontanelle shape the following feature measurements are retained:

- Antero-posterior arc

Specimen	Identificator	Age	Sex
1891-92-83-167	167	0y	F
1892-93-289a-189	189	foetus 9m	I
1892-93-289b-190	190	foetus 7m	I
1892-93-308-199	199	1y	F
1892-93-311-200	200	9m	M
1893-94-6-208	208	2y	F
1893-94-24-215	215	7m	M
1893-94-56-226	226	2m	F
1893-94-73-232	232	13m	M
1893-94-84-238	238	1y	I
1893-94-107-245	245	0y	F
1894-95-27-249	249	0y	M
1894-95-118-274	274	1y7m	M
1894-95-162-282	282	11m	M
1896-97-13-317	317	7m15d	F
1896-97-78-(328)	328	18m	F
1897-98-148-382	382	9m	F
1897-98-150-384	384	2y1m	F
1897-98-165-389	389	2y6m	F
1898-99-128-435	435	0y	M
1898-99-129-436	436	0y	F
1898-99-150-443	443	10d	M
1898-99-231-475	475	2y	F
1901-51-562	562	2y	F
1901-142-571	571	1m15d	M
1902-50-576	576	7m	F
1902-03-53-577	577	1y3m	F
1902-55-579	579	0y	I
1902-59-583	583	3m	F
1902-60-584	584	2m	F
1902-03-111-589	589	4m15d	M
1902-03-113-591	591	2y6m	M
1902-03-128-592	592	2y6m	M
1903-04-19-598	598	2y	M
1904-54-614	614	2y	M
1921-1978-1791	1791	9m(dental)	I
Crâne vitrine 0y	CV0	0y	I
Crâne vitrine 1y	CV1	1y	I
Spockinou	Spk	0y(dental)	I
Maurice	Mac	2y6m(dental)	I

Table 1: Strasbourg juvenile collection: age and sex data.

Age	Sex		
	F	M	I
< 0 year	0	0	2
0 year $\leq$ age < 0.5 year	6	5	3
0.5 year $\leq$ age < 1 year	3	3	1
1 year $\leq$ age < 1.5 years	2	1	2
1.5 years $\leq$ age < 2 years	1	1	0
2 years $\leq$ age < 2.5 years	4	2	0
2.5 years $\leq$ age < 3 years	1	2	1

Table 2: Studied sample of the Strasbourg juvenile collection : age distribution.

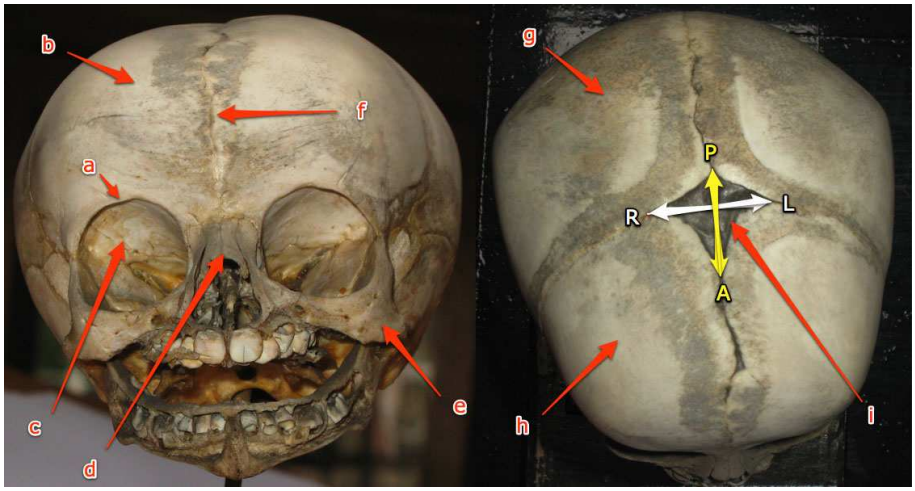

Figure 1: Specimen "CV0" (a) Supra orbital margin (b) Squama (c) Orbital plate (d) Nasal part (e) Zygomatic processes (f) Metopic suture (g) Parietal bone (h) Frontal bone (i) Anterior fontanelle.

The antero-posterior arc is the arc between the points A and P resp. the "antero-most" and the "posterior-most" extremities of the membranous gap along the axe delimiting the contact between the right and the left halves of the skull. The illustration is given in Fig. 1. The length of the antero-posterior arc is also measured manually with a millimeter band along the skull surface.

- Transverse arc

  As shown in Fig. 1, the transverse arc corresponds to the arc between the points R and L resp. The rightmost and the leftmost extremities of the membranous gap along the axe delimiting the contact between the parietal and the frontal bones. The length of the transverse arc is measured manually with a millimeter band along the skull surface.

- Antero-posterior chord

  The antero-posterior chord is the straight line joining the ends of the antero-posterior arc. The length of the antero-posterior chord is also measured manually with an electronic caliper.

- Transverse chord

  The transverse chord is the straight line joining the ends of the transverse arc. The length of the transverse chord is measured manually with an electronic caliper.

- Lateral arcs

  In order to evaluate the anterior fontanelle shape as a whole, arc distances between the points R, P, L and A are measured manually with a millimeter band along the skull surface.

3.2 Manual morphometric evaluation

The morphometric study of the anterior fontanelle consists in arc and chord length evaluation along the antero-posterior axis, the transverse axis and the lateral fontanelle diamond sides. It should be noticed that the reported results are strongly related to the inter-observer variability of the measurements.

3.2.1 Antero-posterior and the transverse arcs

Measures of the antero-posterior and the transverse arcs are summed up in Table 3. The measures are performed with a millimeter band and values are given in centimeters. Each measure is performed by three human operators denoted as bd, pd and sg. Standard deviations of manual arc measures are provided for both arcs AP and RL, denoted as $StdevAP$ and $StdevRL$.

Standard deviations of the inter-observer manual arc measures are also illustrated in Fig. 2. The values of $StdevAP$ (left) and $StdevRL$ (right) are given in centimeters along the vertical axis while along the horizontal axis the specimens are enumerated.

Sp. Id.	AP			Stdev AP	RL			Stdev RL
	[bd] cm	[pd] cm	[sg] cm		[bd] cm	[pd] cm	[sg] cm	
167	1,8	2	2,38	0,29	2,25	2,1	2,38	0,14
189	2,1	2	2,2	0,1	1,5	1,5	1,55	0,03
190	2,9	2,6	2,8	0,15	2	2	2	0
199	3,3	3,3	3,35	0,03	3,3	3,3	3,35	0,03
200	4,3	4	4,55	0,28	4,1	4,3	4,2	0,1
208	2,4	2,5	3,25	0,46	2,6	2,7	2,85	0,13
215	2,6	2,6	2,68	0,04	2,4	2,2	2,45	0,13
226	4	4,1	4,05	0,05	3,7	3,6	3,85	0,13
232	7,4	7,1	6,35	0,54	7,1	6,6	5,9	0,6
238	2,3	2,4	2,55	0,13	2,8	2,8	2,65	0,09
245	1,7	1,1	2,25	0,58	1,5	1,4	1,75	0,18
249	3,6	3,7	3,6	0,06	2,5	2,6	2,63	0,07
274	3,7	3,7	3,7	0	3,8	3,9	4,05	0,13
282	3,75	3,8	4,05	0,16	4,8	4,7	5,15	0,24
317	5,7	5,5	5,68	0,11	4,2	4,2	4,85	0,38
328	1,8	1,8	1,17	0,36	1,5	1,6	1,5	0,06
382	4,25	4,2	4,38	0,09	5,3	5,3	6,1	0,46
384	0,65	0,6	1	0,22	1,05	1,2	1,3	0,13
389	0,6	1,9	1	0,67	1,9	0,7	2,25	0,81
435	4,6	4,4	4,88	0,24	2,85	2,8	2,83	0,03
436	1	1	1,1	0,06	1	1,1	1,1	0,06
443	3,9	3,9	4	0,06	3,2	3,2	3,6	0,23
475	0,15	0,2	0,55	0,22	0,5	0,5	0,7	0,12
562	0,4	0,4	0,5	0,06	0,5	0,45	0,45	0,03
571	3,2	3,2	3,68	0,27	3,5	3,5	3,65	0,09
576	4,55	4,6	4,6	0,03	4,2	4	4,2	0,12
577	3	3,2	3,25	0,13	3,7	3,7	3,75	0,03
579	4,6	4,5	4,5	0,06	3,1	3,1	3,3	0,12
583	3,85	3,8	3,9	0,05	3,6	3,6	3,68	0,04
584	4,3	4,2	4,4	0,1	2,75	2,9	2,88	0,08
589	5,1	5	5,05	0,05	4,9	4,9	5,18	0,16
591	1,15	1,2	1,43	0,15	1,9	1,9	2	0,06
592	1,9	1,9	2,3	0,23	3,3	3,3	3,64	0,19
598	2,7	2,8	2,75	0,05	3,3	3,3	3,4	0,06
614	0,7	0,3	1,3	0,5	0,25	0,2	0,45	0,13
1791	5,1	5	5,63	0,34	3,8	3,8	3,9	0,06
CV0	3	3,1	4,6	0,9	3	3,1	3,43	0,22
CV1	5,4	5,1	5,2	0,15	4,5	4,6	4,4	0,1
Spk	6,6	6	6,75	0,4	5	4,9	5,7	0,44
Mac	1,4	1,6	1,55	0,1	2,4	2,3	2,05	0,18

Table 3: Inter-observer manual measures of AP and RL arcs.

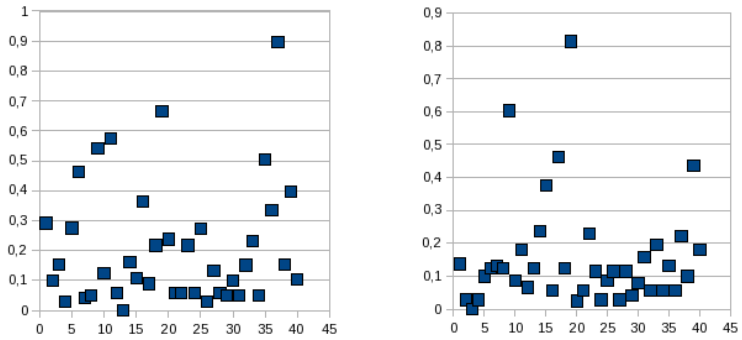

Figure 2: Standard deviations of inter-observer manual measures of AP (left) and RL (right) arcs.

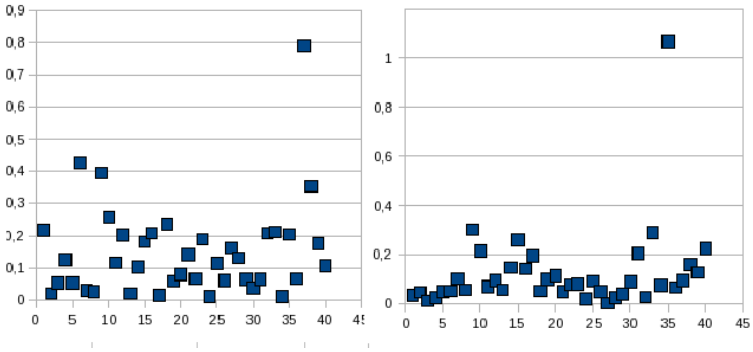

Figure 3: Standard deviations of inter-observer manual measures of: AP (left) and RL (right) chords.

3.2.2 Antero-posterior and the transverse chords

The antero-posterior and the transverse chord measurements are given in Table 4.

Standard deviations of the inter-observer manual chord measures are also illustrated in Fig. 3. The values of *StdevAP* (left) and *StdevRL* (right) are given in centimeters along the vertical axis while along the horizontal axis the specimens are enumerated.

3.2.3 Lateral arcs

The lateral arcs along the sides of the diamond shaped fontanelle are given in Table 5.

In some cases the fontanelle is almost closed, abbreviated *a.c.*, as for example

Sp. Id.	AP				Stdev AP	RL				Stdev RL
	[hc] cm	[hcb] cm	[sg] cm	[sgb] cm		[hc] cm	[hcb] cm	[sg] cm	[sgb] cm	
167	1,69	1,9	1,75	2,18	0,22	2,21	2,28	2,27	2,28	0,03
189	1,91	1,91	1,94	1,89	0,02	1,43	1,43	1,45	1,53	0,05
190	2,53	2,53	2,64	2,57	0,05	1,94	1,94	1,93	1,91	0,01
199	3,57	3,33	3,34	3,3	0,12	3,26	3,26	3,31	3,27	0,02
200	4,39	4,34	4,43	4,46	0,05	4,02	4,13	4,12	4,09	0,05
208	2,5	2,46	3,19	3,25	0,43	2,67	2,65	2,77	2,68	0,05
215	2,62	2,67	2,69	2,69	0,03	2,2	2,17	2,38	2,33	0,1
226	4,02	4,02	4,05	4,07	0,03	3,31	3,31	3,2	3,33	0,06
232	7,26	7,12	6,45	6,57	0,4	6,4	6,58	5,93	6,05	0,3
238	2,31	2,88	2,4	2,41	0,26	2,3	2,82	2,6	2,62	0,21
245	1,94	1,76	1,71	1,68	0,12	1,51	1,5	1,36	1,44	0,07
249	3,33	3,33	3,61	3,73	0,2	2,32	2,32	2,47	2,49	0,09
274	3,65	3,68	3,67	3,63	0,02	4,02	3,93	3,89	3,91	0,06
282	3,75	3,89	4	3,93	0,1	4,62	4,55	4,87	4,79	0,15
317	5,85	5,85	5,57	5,51	0,18	4,36	4,36	4,73	4,87	0,26
328	1,76	1,67	1,33	1,41	0,21	1,67	1,53	1,43	1,34	0,14
382	4,26	4,26	4,29	4,29	0,02	5,39	5,39	5,71	5,74	0,19
384	0,64	0,62	1,05	1,02	0,23	1,21	1,27	1,22	1,32	0,05
389	0,72	0,72	0,84	0,73	0,06	1,99	1,99	2,2	2,11	0,1
435	4,4	4,48	4,54	4,58	0,08	3,06	2,85	2,8	2,87	0,11
436	1,31	1,07	1,02	1,02	0,14	0,95	1	1,07	1,01	0,05
443	3,67	3,78	3,81	3,81	0,07	2,78	2,91	2,94	2,94	0,08
475	0,24	0,24	0,6	0,53	0,19	0,56	0,56	0,66	0,72	0,08
562	0,46	0,46	0,45	0,48	0,01	0,47	0,47	0,45	0,43	0,02
571	3,25	3,09	3,13	3,34	0,11	3,47	3,48	3,66	3,47	0,09
576	4,62	4,55	4,61	4,49	0,06	4,08	4	4,12	4,05	0,05
577	2,73	2,9	3,07	3,06	0,16	3,56	3,56	3,56	3,56	0
579	4,49	4,49	4,21	4,41	0,13	3	3	3,04	2,98	0,02
583	3,88	3,76	3,86	3,77	0,06	3,56	3,58	3,52	3,49	0,04
584	4,24	4,31	4,23	4,25	0,04	2,81	2,77	2,66	2,62	0,09
589	5,02	4,93	4,93	4,87	0,06	4,44	4,75	4,83	4,9	0,2
591	1,21	1,1	1,46	1,54	0,21	1,93	1,9	1,94	1,96	0,03
592	2,24	1,94	2,43	2,33	0,21	3,39	3,26	3,36	3,91	0,29
598	2,79	2,76	2,78	2,77	0,01	3,15	3,3	3,31	3,24	0,08
614	0,73	0,73	1,03	1,12	0,2	2,28	2,28	0,42	0,44	1,07
1791	5,09	5,08	5,04	4,94	0,07	3,66	3,74	3,73	3,82	0,07
CV0	3,19	3,19	4,52	4,59	0,79	3,05	3,05	3,13	3,25	0,09
CV1	5,26	5,26	5,96	5,24	0,35	4,4	4,4	4,46	4,74	0,16
Spk	6,36	6,36	6,66	6,66	0,17	4,78	4,78	5	5	0,13
Mac	1,55	1,55	1,33	1,54	0,11	2,41	2,41	1,98	2,07	0,22

Table 4: Inter-observer manual measures of AP and RL chords.

Sp. Id.	AR (M1)		Stdev	RP (M2)		Stdev	PL (M3)		Stdev	LA (M4)		Stdev
	[sg] cm	[sgb] cm	M1	[sg] cm	[sgb] cm	M2	[sg] cm	[sgb] cm	M3	[sg] cm	[sgb] cm	M4
167	2,6	2,5	0,07	1,4	1,75	0,25	1,25	1,25	0	2,2	2,5	0,21
189	2	2	0	1	1	0	0,7	0,7	0	1,6	1,5	0,07
190	2,5	2,7	0,14	1,3	1,25	0,04	1	1	0	2,6	2,6	0
199	3,2	3,1	0,07	2	2,2	0,14	2	1,9	0,07	2,9	2,8	0,07
200	3,5	4	0,35	2,7	2,7	0	2,7	2,6	0,07	3,7	3,7	0
208	2,6	2,5	0,07	1,7	2	0,21	1,7	1,7	0	3,5	3,7	0,14
215	3	2,7	0,21	1,5	1,25	0,18	2,1	2,1	0	2,7	2,6	0,07
226	3,8	3,5	0,21	3	3	0	2,2	2,5	0,21	4	3,8	0,14
232	5,8	5,61	0,13	3,5	3,5	0	3,6	3,8	0,14	6,6	6,6	0
238	2,3	2,25	0,04	1,6	1,8	0,14	1,35	1,4	0,04	2,4	2,2	0,14
245	1,7	1,7	0	0,8	1,1	0,21	1,2	1,2	0	2	1,9	0,07
249	3,75	4,1	0,25	1,6	1,5	0,07	1,4	1,6	0,14	3,25	3,5	0,18
274	3	2,8	0,14	2,5	2,6	0,07	2,7	2,7	0	3,2	3,2	0
282	5	4,8	0,14	4,25	4	0,18	2,4	2,25	0,11	3,4	3,7	0,21
317	5,25	5,6	0,25	2,7	2,8	0,07	2,7	2,8	0,07	5,3	5,3	0
328	1,75	1,75	0	1,1	1,1	0	1	1	0	1,25	1,25	0
382	4,8	4,7	0,07	3,8	3,7	0,07	3,1	3	0,07	4,6	4,7	0,07
384	e.											
389	a.c.											
435	4,3	4,5	0,14	2	1,8	0,14	1,8	1,7	0,07	3,7	3,7	0
436	1,1	1,1	0	0,7	0,7	0	0,5	0,5	0	0,7	0,7	0
443	4,3	4,3	0	2,7	2,7	0	2,2	2,2	0	4,3	4,3	0
475	a. c.											
562	a. c.											
571	a. c.											
576	3,7	3,6	0,07	2,6			2,6	2,6	0	4,1	4,2	0,07
577	3	2,8	0,14	2,3	2,4	0,07	1,8	2,2	0,28	3,1	3,3	0,14
579	4,1	4,1	0	1,7	1,7	0	2,2	2,2	0	4,2	4,2	0
583	3,8	3,5	0,21	2,2	2,3	0,07	2,3	2,5	0,14	3,5	3,8	0,21
584	4,1	4,1	0	1,75	1,6	0,11	2	2	0	4,2	4,1	0,07
589	4,5	4,8	0,21	3	3,1	0,07	2,8	2,9	0,07	5,1	5,3	0,14
591	1	1	0	1,5	1,2	0,21	1,1	1,1	0	1,3	1,3	0
592	2,8	2,8	0	2,5	2,6	0,07	1,8	1,8	0	2,5	2,6	0,07
598	2,1	2,1	0	2,5	2,5	0	2,2	2,2	0	2,2	2,3	0,07
614	a. c.											
1791	4,75	4,4	0,25	2,8	3	0,14	2,5	2,5	0	5,2	5	0,14
CV0	4,8	5	0,14	1,7	1,8	0,07	1,5	1,75	0,18	4,5	4,9	0,28
CV1	6	6	0	4,5	4,5	0	5	5	0	6,5	6	0,35
Spk	5,2	5,5	0,21	4,5	4,5	0	4,3	4,3	0	6	5,8	0,14
Mac	2,2	2,2	0	1,4	1,6	0,14	1,1	1,1	0	2,3	2	0,21

Table 5: Intra-observer manual measures of fontanelle lateral side arcs.

the specimens 475 and 562. The fontanelle could be also ellipse like, abbreviated *e.*, as for example the specimen 384. For such specimens no lateral side arcs could be measured. It should be noticed that the given values are intra-observer measurements. That is why the standard deviations are often zero valued.

3.2.4 Discussion

Let us analyse results illustrated in Table 3 and Table 4.

The following observations can be made:

- Standard deviation for the AP manual arc measures is in the range of $[0,00; 0,90]cm$.
- Standard deviation for the RL manual arc measures is in the range of $[0,00; 0,81]cm$.
- The worst results for the AP and RL manual arc measures are resp. for the specimens $CV0$ and 389. Looking at the photo of the specimen $CV0$ given in appendix H, Fig.1, one can see that the fontanelle has a singular stretched shape along the AP axis that leads to various evaluation according to the human operators. The specimen 389, see appendix D, Fig.3, has an almost closed fontanelle that makes difficult the morphometric evaluation.
- Standard deviation for the AP manual chord measures is in the range of $[0,01; 0,79]cm$.
- Standard deviation for the RL manual chord measures is in the range of $[0.00; 1,07]cm$.
- The worst results for the AP and RL manual chord measures are resp. for the specimens $CV0$ and 614. As remarked above $CV0$ given in appendix H, Fig.1, has an AP axis stretched shape that misleads evaluation. While, the fontanelle of the specimen 614, see appendix G, Fig.3, is almost closed thus invalidating the morphometric evaluation.
- Chord measures are more precise than the arc ones. Indeed, according to our experience it is very difficult to position the millimeter band on the skullcap surface. Often, the skullcap is damaged, moreover the anterior fontanelle is a gap in the surface and thus the surface curvature evaluation over it is roughly approximated.
- The threshold of `0,3cm` of the *Stdev* emerged as a good confidence interval approximation for both arc and chord manual morphometric evaluation. For the arc measures `80%` of the evaluated features do not exceed this threshold while for chord measures the population under this threshold is `91,2%`.

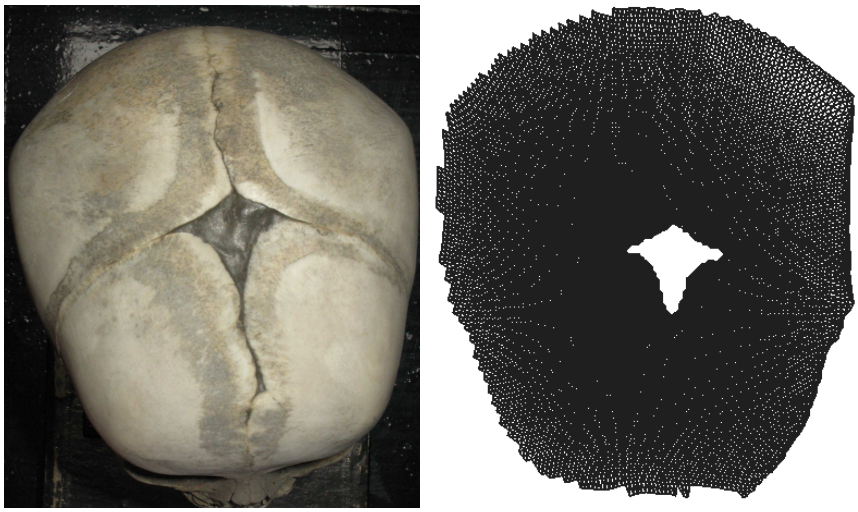

Figure 4: Specimen "CV0": original (left) and numerical model (right).

Let us analyse results illustrated in Fig. 2 and in Fig. 3. One can see that both arc and chord measures along the medio-lateral axis are more stable and accurately evaluated than the ones along the antero-posterior axis. Furthermore, one reason for the outcoming uncertainty in inter-observer measurements is that the anterior fontanelle margins are often uncomplete and could vary depending on the subjective human operator evaluation. See for example the specimen 199 given in appendix A, Fig.4. A solution to this problem is to make as much as possible reproducible the measurement protocol. The measurements should be done with the same measurement tools and by at least two human operators.

4 Data acquisition and reconstruction: material and methods

4.1 Experimental platform

Our experimental platform is based on a low cost portable 3D laser scanner, the Minolta VIVID300. The basic advantage of this device is the greatly facilitated 3D model acquisition as well as the fact that this scanner is easily transferred in altered circumstances for the study of specimen collections "in situ" in the museums and thus preserving the exhibition original pieces. The drawback of this acquisition device is the limited acquisition resolution that necessitates a more careful post processing of the reconstructed mesh models. This post processing, all the numerical measures and the visualisation are performed on an Intel Pentium4, 3GHz, 1Go RAM using our own software package [12].

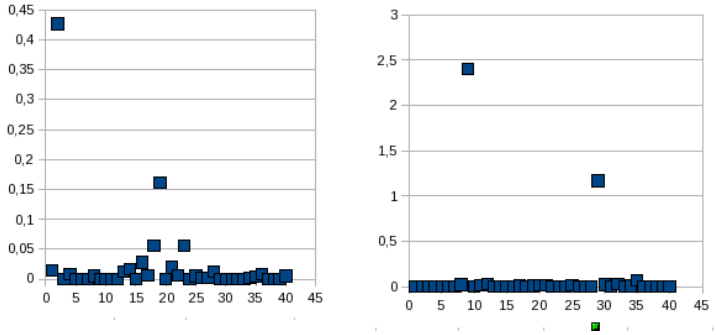

Figure 5: Standard deviations of inter-observer numerical measures of: AP (left) and RL (right) chords.

4.2 Digital morphometric analysis: numerical morphometric evaluation of the anterior fontanelle

As a result of our acquisition and reconstruction pipeline, numerical models of the anterior fontanelle for the osteological Strasbourg collection are produced. An illustration of the produced mesh model for the specimen `CV0` is given in Fig. 4.

4.2.1 Numerical evaluation of the antero-posterior and the transverse chords

On the next stage of the processing, `AP` and `LR` chords are measured as euclidean distances between representative vertices of the supported triangular mesh models. Each representative vertex is situated in a vertex from the skull mesh model corresponding to the chosen landmark position. Inter-observer numerical measurements of the `AP` and `LR` chords are performed and their standard deviations, $StdevAP$ and $StdevLR$, are given in Table 6.

Standard deviations of the inter-observer numerical chord measures are also represented in Fig. 5. Along the vertical axis $StdevAP$ and $StdevLR$ are given in centimeters while along the horizontal axis the specimens are enumerated.

4.2.2 Discussion

According to the results given in Table 6 and Fig. 5 the following observations are made:

- Standard deviation for the numerical measures of the AP chords is in the range of $[0,00; 0,16]cm$.
- Standard deviation for the numerical measures of the RL chords is in the range of $[0,00; 0,03]cm$.

Sp. Id.	AP			Stdev AP	RL			Stdev RL
	[rs] cm	[hc] cm	[bd] cm		[rs] cm	[hc] cm	[bd] cm	
167	2,19	2,21	2,19	0,01	2,03	2,05	2,03	0,01
189	1,43	1,43	1,43	0	1,81	1,81	1,81	0
190	1,93	1,93	1,93	0	2,5	2,51	2,51	0,01
199	3,18	3,2	3,2	0,01	3,61	3,61	3,61	0
200	4,13	4,13	4,13	0	4,39	4,39	4,39	0
208	2,54	2,54	2,54	0	2,02	2,02	2,02	0
215	1,95	1,95	1,95	0	2,51	2,51	2,51	0
226	3,61	3,62	3,61	0,01	4,5	4,54	4,5	0,02
232	6,2	6,2	6,2	0	6,58	6,58	6,58	0
238	2,39	2,39	2,39	0	2,34	2,34	2,34	0
245	1,44	1,44	1,44	0	1,39	1,41	1,37	0,02
249	2,36	2,36	2,36	0	3,5	3,44	3,46	0,03
274	4,11	4,08	4,09	0,01	4,04	4,04	4,04	0
282	3,19	3,22	3,22	0,02	3,63	3,63	3,64	0,01
317	4,25	4,25	4,25	0	5,8	5,8	5,8	0
328	1,33	1,34	1,38	0,03	1,22	1,22	1,22	0
382	3,88	3,87	3,87	0,01	3,86	3,86	3,88	0,01
384	1,3	1,24	1,19	0,06	0,94	0,94	0,94	0
389	2,37	2,65	2,65	0,16	0,65	0,64	0,64	0,01
435	2,71	2,71	2,71	0	3,83	3,81	3,83	0,01
436	0,61	0,58	0,58	0,02	0,79	0,79	0,75	0,02
443	2,14	2,13	2,14	0,01	2,84	2,85	2,84	0,01
475	0,73	0,73	0,63	0,06	0,49	0,49	0,48	0,01
562	0,52	0,52	0,52	0	0,44	0,43	0,43	0,01
571	3,1	3,09	3,09	0,01	3,63	3,59	3,59	0,02
576	3,85	3,85	3,85	0	4,56	4,57	4,56	0
577	3,4	3,4	3,4	0	2,9	2,9	2,9	0
579	3	3,01	2,99	0,01	3,8	3,8	3,79	0
583	3,45	3,45	3,45	0	3,72	3,71	3,72	0
584	2,59	2,59	2,59	0	4,27	4,27	4,23	0,03
589	4,59	4,59	4,59	0	4,78	4,78	4,78	0
591	1,99	1,99	1,99	0	1,28	1,25	1,21	0,03
592	3,73	3,73	3,73	0	2,12	2,12	2,12	0
598	3,16	3,17	3,17	0	2,89	2,9	2,88	0,01
614	0,44	0,44	0,44	0	0,46	0,45	0,45	0,01
1791	3,97	3,99	3,97	0,01	5,37	5,37	5,37	0
CV0	2,68	2,68	2,68	0	2,48	2,48	2,48	0
CV1	4,72	4,72	4,72	0	6,06	6,06	6,06	0
Spk	4,84	4,84	4,84	0	6,01	6,01	6,01	0
Mac	2,57	2,56	2,56	0,01	1,41	1,41	1,41	0

Table 6: Inter-observer numerical measures of AP and RL chords.

- The worst results are for the specimens 389 and 614 shown resp. in appendix D, Fig.3, and appendix G, Fig.3. As one can see anterior fontanelles of these specimens have singular shapes leading to ambiguous interpretations.

- The confidence interval is much tighter for the numerical morphometric evaluations than the manual ones: the `Stdev` of `95,6%` of the specimen population is under `0,16cm`.

- The `RL` chord measures are more precise than the `AP` chord measures similarly to the manual measures.

- The numerical model allows a more reliable landmark position identification.

4.3 Correlation between manual and numerical morphometric evaluation

In order to evaluate the correlation between the manual and the numerical measures, numerically calculated values are added as complementary observations of a "virtual operator". The resulting standard deviations of the manual, the numerical and the mixed measure series for the AP and RL chords are given in Table 7.

One observes that:

- Standard deviation range intervals for manual and "mixed" observations remain comparables, see Fig. 6. For AP chord mixed measures it is in the range of $[0,03; 0,97]$ while for RL chord mixed measures standard deviation is in the range of $[0,02; 0,92]$.

- The cases where the difference between the standard deviations of the manual measures and the mixed measures is great than $0.5cm$ are singular. See for instance the specimen 389 having the maximal deviation between manual and mixed measures for the chord AP. As noticed before for this specimen the fontanelle is almost closed. By similitude, the specimen 1791, appendix G, Fig.4, has the maximal deviation between manual and mixed measures for the chord RL. Again looking to the original, it is discerned that the protection folio spreaded over the anterior fontanelle provokes misleading numerical acquisitions.

According to these observations it could be deduced that numerical measures as a whole do not deteriorate anterior fontanelle size evaluation. Moreover, they are independant from the human factor and preserves the integrity of the studied osteological material.

Sp. Id.	Stdev AP			Stdev RL		
	manual	numerical	mixed	manual	numerical	mixed
167	0,22	0,01	0,23	0,03	0,01	0,12
189	0,02	0	0,26	0,05	0	0,19
190	0,05	0	0,34	0,01	0,01	0,31
199	0,12	0,01	0,14	0,02	0	0,18
200	0,05	0	0,15	0,05	0	0,16
208	0,43	0	0,34	0,05	0	0,36
215	0,03	0	0,38	0,1	0	0,15
226	0,03	0,01	0,23	0,06	0,02	0,66
232	0,4	0	0,45	0,3	0	0,28
238	0,26	0	0,19	0,21	0	0,2
245	0,12	0	0,2	0,07	0,02	0,06
249	0,2	0	0,63	0,09	0,03	0,57
274	0,02	0,01	0,23	0,06	0	0,07
282	0,1	0,02	0,37	0,15	0,01	0,58
317	0,18	0	0,78	0,26	0	0,68
328	0,21	0,03	0,18	0,14	0	0,18
382	0,02	0,01	0,22	0,19	0,01	0,92
384	0,23	0,06	0,28	0,05	0	0,17
389	0,06	0,16	0,97	0,1	0,01	0,77
435	0,08	0	0,96	0,11	0,01	0,5
436	0,14	0,02	0,29	0,05	0,02	0,13
443	0,07	0,01	0,87	0,08	0,01	0,06
475	0,19	0,06	0,21	0,08	0,01	0,09
562	0,01	0	0,03	0,02	0,01	0,02
571	0,11	0,01	0,1	0,09	0,02	0,08
576	0,06	0	0,39	0,05	0	0,27
577	0,16	0	0,27	0	0	0,35
579	0,13	0,01	0,75	0,02	0	0,42
583	0,06	0	0,2	0,04	0	0,1
584	0,04	0	0,89	0,09	0,03	0,83
589	0,06	0	0,19	0,2	0	0,15
591	0,21	0	0,38	0,03	0,03	0,37
592	0,21	0	0,81	0,29	0	0,75
598	0,01	0	0,21	0,08	0,01	0,2
614	0,2	0	0,29	1,07	0,01	0,9
1791	0,07	0,01	0,57	0,07	0	0,88
CV0	0,79	0	0,85	0,09	0	0,35
CV1	0,35	0	0,45	0,16	0	0,84
Spk	0,17	0	0,9	0,13	0	0,6
Mac	0,11	0,01	0,58	0,22	0	0,46

Table 7: Standard deviations of the inter-observer manual, numerical and mixed measures of AP and RL chords.

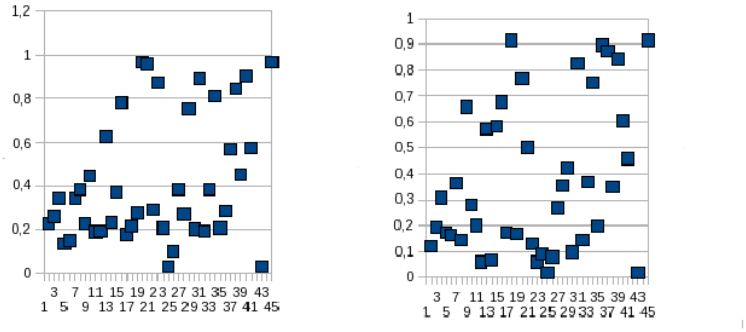

Figure 6: Standard deviations of inter-observer mixed measures of: AP (left) and RL (right) chords.

5 Reproduction and validation of the results

In order to validate the digital analysis, numerically calculated distances are compared with their manual counterparts. For the moment, only the similarity of the `AP` and `RL` chord measures is exploited. In `78,2%` of the specimen population the `Stdev` between manual and numerical length measures is under `0,5cm`. In almost all cases with `Stdev` out of this range the numerical estimation error is owed to damaged original skull surface that mislead the laser scan acquisition and thus the posterior object reconstruction. This results gives us the opportunity to further exploit the digital analysis using 3D impressions of the initial shapes. According to our experience the minimal thickness of printable offset surfaces corresponding to numerical representations of the osteological surfaces are within the same range ie `0,5cm`.

6 Conclusion

Feature definition is a primordial factor in object retrieval. Depending on its size, shape and position on the object, the data acquisition process could produce invalid results. Furthermore, the validation of the object reconstruction is determined on the ability to perform reliable morphometric measures.

For the study of the anterior fontanelle we intend to include additional numerical measurements of the fontanelle side arcs.

Moreover we envisage to develop tools for repairing the reconstructed mesh model as the constrained hole filling that maintain surface curvature.

Digital morphometric analysis is in a "premature" stage as long as it is strongly related to the measurement error control all over the acquisition and reconstruction pipeline. 3D object reconstruction becomes an integral part of

Figure 7: From left to right: Hélène, Pr. Khan, Bruno, Mr. Leman.

current computer graphics applications but the development of efficient retrieval methods with certified reconstruction error range remains a challenge.

7 Appendices

7.1 Acknowledgments

`Acknowledgments`
The authors thank Pr. Jean-Luc Khan for access and help with Strasbourg collection and Dr. Hélène Coqueugniot for valuable technical support.
The authors thank Mr. Leman for access and animation. The commented visit of the institute private underground collection leaved unforgettable memories.

7.2 Research team

- LaBRI Laboratoire Bordelais de Recherche en Informatique, UMR 5800 CNRS, Université Bordeaux 1, 351 Cours de la Libération, 33405 Talence. Pascal Desbarats, Stefka Gueorguieva and Remi Synave are members of LaBRI working in the team "Image and Sound". For almost ten years, medical image processing is a priority domain in the scientific and teaching activities of the team members. Multiple competences as image processing, geometric modeling, visualisation and 3D interaction, video analysis, data indexation and multimedia, are promoted in order to develop computer assisted design and engineering of anatomical shapes.

- LAPP Laboratoire d'Anthropologie des Populations du Passé, UMR 5199-PACEA, Université Bordeaux 1, avenue des Facultés, 33405 Talence. Hélène Coqueugniot and Bruno Dutailly are members of LAPP.
  Within the LAPP for several years researches in the field of medical image processing and 3D morphometry have been engaged. On one hand, thin anatomical structures are investigated and thus necessitate acquisition and reconstruction precision in the range of 0,1cm. On the other

Figure 8: From left to right: Pascal, Stefka and Remi.

hand, the increasingly powerful data processing tools of image segmentation and analysis allow revision and further extension of known theories and hypotheses as the relation of the anterior fontanelle size to sex, head circumference or bone age.

7.3 Studied sample of specimens

- Appendix A: No 167,189,190,199, 200 and 208.
- Appendix B: No 215, 226, 232, 238 and 245.
- Appendix C: No 249, 274, 282, 317 and 328.
- Appendix D: No 382, 384, 389, 435 and 436.
- Appendix E: No 443, 475, 562, 571 and 576.
- Appendix F: No 577, 583, 584, 589 and 591.
- Appendix G: No 592, 598, 614 and 1791.
- Appendix H: No CV0, CV1, Spk and Mac.

References

[1] D.C. Adams. Geometric morphometrics: Ten years of progress following the 'revolution'. *Italian Journal of Zoology*, (71):5–16, 2004.

[2] H. Coqueugniot. Le crâne d'*Homo sapiens* en eurasie: croissance et variation depuis 100 000 ans. *British Archeological Reports, International Series*, 822, 1999.

[3] H. Coqueugniot. Collection ostéologique immature. Technical report, Institut d'anatomie normale de Strasbourg. Faculté de médecine, 2000.

[4] H. Coqueugniot, J.-J. Hublin, F. Veillon, F. Houet, and T. Jacob. Early brain growth in *Homo erectus* and implications for cognitive ability. *Nature*, 431, 2004.

[5] K. Hildebrandt, K. Polthier, and M. Wardetzky. On the convergence of metric and geometric properties of polyhedral surfaces. In *Research Report 05-24*, 2005.

[6] K. Polthier, M. Schmies, M. Steffens, and Ch. Teitzel. The video "geodesics and waves". In *Symposium on Computational Geometry*, pages 411–412, 1999.

[7] M. Rampont. *Les squelettes, os et dents de foetus, nouveaux-né et enfants du musée anatomique de Strasbourg. Aspect historiques et catalogues.* Thèse de médecine No 192, Université Louis Pasteur Strasbourg 1, 1994.

[8] S. Rusinkiewicz, O.A. Hall-Holt, and M. Levoy. Real-time 3d model acquisition. In *SIGGRAPH*, pages 438–446, 2002.

[9] L. Scheuer and S. Black. *Developmental Juvenile Osteology.* Elsevier Academic Press, 2000.

[10] D.E. Slice. *Modern Morphometrics in Physical Anthropology.* Kluwer Academic Plenium Publishers, 2005.

[11] V. Surazhsky, T. Surazhsky, D. Kirsanov, S.J. Gortler, and H. Hoppe. Fast exact and approximate geodesics on meshes. *ACM Trans. Graph.*, 24(3):553–560, 2005.

[12] R. Synave, P. Desbarats, and S. Gueorguieva. Toolkit for registration and evaluation for 3d laser scanner acquisition. In *WSCG'2008*, pages 199–204, Plzen: University of West Behemia, February 2008.

[13] R. Synave, S. Gueorguieva, and P. Desbarats. Constraint shorthest path computation on polyhedral surfaces. Technical Report RR-1447-08, LaBRI, UMR 5800, 2008.